Oxid Met (2018) 90:135–151
https://doi.org/10.1007/s11085-017-9828-z

ORIGINAL PAPER

Dependence on the Chromium Content of the High-Temperature Oxidation Behavior of Ta-Rich Nickel-Based Cast Alloys

Patrice Berthod[1,2] · **Zohra Himeur**[1]

Received: 30 September 2017 / Revised: 30 November 2017 / Published online: 16 December 2017
© Springer Science+Business Media, LLC, part of Springer Nature 2017

Abstract The high-temperature stability of primary tantalum carbides is a problem of importance for chromium-rich cast alloys, based on cobalt or nickel. The focus of this study was nickel-based alloys, as these alloys are particularly sensitive to a lack of TaC in the as-cast state and by dissolution due to high-temperature exposure. In this work, a possible way for promoting the formation of many TaC precipitates by changing from the usual 30 wt% chromium content was investigated. Five alloys with Cr content varying from 10 to 50 wt% were prepared and then subjected to microstructure characterization and to oxidation tests. In contrast with what was expected, decreasing the Cr content in comparison with the Ni–30Cr–0.4C–6Ta reference alloy did not succeed in obtaining more TaC precipitates, but instead had the opposite effect. Concerning the high-temperature oxidation behavior at 1127 and 1237 °C, loss of resistance was observed only for a Cr content at the lower level of 10 wt%. It was noticed that a subscale $CrTaO_4$ developed during oxidation and seemed to promote oxide spallation during cooling.

Keywords Cast nickel-based alloys · High tantalum content · Varying chromium content · High temperature oxidation

✉ Patrice Berthod
patrice.berthod@centraliens-lille.org

Zohra Himeur
himeurzahra@gmail.com

[1] Faculty of Science and Technologies, University of Lorraine, Postal Box 70239, 54506 Vandoeuvre-lès-Nancy, France

[2] Department CP2S, CNRS, Institut Jean Lamour (UMR 7198), University of Lorraine, Postal Box 70239, 54506 Vandoeuvre-lès-Nancy, France

Introduction

Chromium is, with aluminum and silicon, one of the three main elements added in rather high quantities in superalloys to allow them resisting oxidation by hot gases in service [1, 2]. In presence of carbon, chromium may also play the role of a carbide-former element. In favorable chemical compositions, it allows obtaining Cr_7C_3 or $Cr_{23}C_6$, the types of chromium carbides which are usually met in superalloys [3, 4]. It is commonly considered that 20 wt%Cr is the low limit for a nickel-based alloy for keeping a chromia-forming behavior on long time when it is exposed at high temperature in oxidant atmosphere [1, 2, 5]. However, chromium may present several disadvantages. One already knows the toxicity problems of the Cr^{VI} specie [6] and the possible re-oxidation of the protective chromia scale into gaseous species [2, 7, 8], notably in the presence of water vapor [9, 13]. But also the presence of chromium in nickel alloys may threaten the thermodynamic stability of the tantalum carbides [14]. This may be a problem since these ones play an important role in the reinforcement of cast superalloys [15], notably in the case of the cobalt-based ones [16]. Indeed, in contrast with some other MC carbides in nickel alloys (e.g., HfC) [17], or with all MC carbides in cobalt-based or iron-based alloys [18, 19], it seems that tantalum carbides exist together with chromium carbides. This is true even for the nickel alloys which are designed to promote the formation of exclusively TaC, i.e., containing as carbon atoms as tantalum atoms. It is maybe possible to favor the development of more TaC in a nickel–chromium alloy by decreasing its chromium content in order to lower the efficiency of this carbide-former competitor. But this needs to be experimentally verified as well as the consequences of this Cr decrease for the behavior of the alloy in oxidation at high temperature. One can fear threats on the oxidation resistance as soon as the Cr content becomes lower than a limit. This limit may perhaps depend on the presence of the significant quantity of tantalum required to obtain TaC volume fractions high enough to achieve efficient mechanical strengthening in case of a success of their stabilization by Cr impoverishment.

In this work, one examines, for a series of {Ni–0.4C–6Ta, wt%}-based alloys, the evolution of the carbides population when the Cr content decreases from the classical 30 wt% value down to 0. One also investigates the consequences of these changes in chromium content on the oxidation behavior at two temperatures which are higher than 1100 °C. This study was also extended to alloys with Cr contents beyond 30 wt%, up to 50 wt%, since it appeared also interesting to explore also the natures of the carbides and the oxidation behavior when the opposite action is done.

Experimental Procedures

Elaboration of the Alloys

A series of five Ni-based alloys was synthesized by induction melting and casting under inert atmosphere. All these alloys contain 0.4 wt%C, 6 wt%Ta and a variable

Cr content. These alloys are different from one another about their chromium content. The Cr content varies from 10 to 50 wt%. The studied alloys are named "NTCxCr," in which x is the weight content in Cr. Their targeted chemical compositions are shown in Table 1. For each alloy, a mix of metallic elements (Ni, Cr, Ta: Alfa Aesar, C: pure graphite) was prepared by targeting a total mass of about 40 g. This mix of pure elements was placed in the water-cooled copper crucible of a CELES (France) furnace. This crucible was surrounded by a silica tube to isolate from air the inert internal atmosphere (300 millibars of pure Ar). The mixed elements were heated until reaching 2.5 kV. This voltage was maintained during 30 s (thermal homogenization). Voltage was then increased until reaching 5 kV. It was maintained for 3 min for achieving total melting and then chemical homogenization. The alloy solidified first time by decreasing the injected power. It was thereafter melted again according to the same cycle, in order to be sure of the total absence of any not-molten parts in the final ingot.

Preparation of the Samples, Oxidation Tests in Furnace and Metallographic Preparation

The obtained ingots were of a compact conic shape. Each of them was divided into four quarters, by using a Buehler Delta Abrasimet metallographic saw. One of these quarters was prepared as a metallographic sample devoted to the control of the as-cast microstructure. Two others were prepared for the high-temperature oxidation tests. These ones were ground all around using 1200-grit SiC papers. A quarter by alloy was exposed at 1127 °C in a resistive furnace (Nabertherm) during 24 h. A second one was exposed at 1237 °C, in the same furnace and in the same atmosphere (laboratory air). After total cooling, the oxidized samples were all coated by cathodic pulverization of gold. This aimed to give a good electrical conductivity to their surface, despite the presence of the oxide scales. A second coating was then electrolytically applied (Ni^{2+} solution heated at 50 °C, 2 h at about 20 mA/cm^2). This led to a sufficiently thick shell of electrolytic Ni for protecting the external oxide scales during cutting. The oxidized samples were thereafter cut into two parts, by using the same metallographic saw as described above. The as-cast parts and the parts of oxidized samples were embedded in a cold resin mixture (ESCIL, France). They were ground with SiC papers of 240 to 1200 grits, water-washed and ultrasonically cleaned. Final polishing was achieved with a {1-μm hard particles}-containing textile disk. The obtained mirror-like samples were thus ready for metallographic characterization.

Table 1 Theoretic compositions for the five studied alloys (weight contents)

Alloys	Ni	Cr	Ta	C
"NCT10Cr"	Bal.	10	6	0.4
"NCT20Cr"	Bal.	20	6	0.4
"NCT30Cr"	Bal.	30	6	0.4
"NCT40Cr"	Bal.	40	6	0.4
"NCT50Cr"	Bal.	50	6	0.4

Bulk, Subsurface and Surface Characterization

A JSM-6010LA scanning electron microscope (SEM) from JEOL (Japan), equipped with an energy dispersion spectrometer (EDS) was used to visualize the as-cast microstructures. Micrographs were taken in back scattered electron (BSE) mode to carry out surface fraction measurements of the different types of carbides present in the bulk. These measurements were done using the image analysis tool of the Photoshop CS software of Adobe. The subsurface microstructure changes due to oxidation were also observed using the SEM in BSE mode, as well as the oxides formed internally and externally. The depths of the subsurface alloy zones which lost their carbides (from the alloy/external oxide interface) were measured. It was also attempted to value the average thickness of the external oxides. Spot EDS analyses were carried out to assess the chemical compositions in the subsurface (concentration profiles), notably in the extreme surface close to the oxidation front. Spot EDS analyses also allowed identifying the nature of all the present oxides.

Results

Microstructures of the Obtained Alloys

The five micrographs presented in Fig. 1 are taken using the SEM in BSE mode. They illustrate the as-cast microstructures of the alloys. The obtained chemical compositions are displayed in Table 2. Concerning the later one, it can be seen that the Cr content is rather well respected for all alloys. This seems to be not the case for tantalum. Indeed, instead to be diminished by possible oxidation during the elaboration as this can be feared by considering the high reactivity of this element, its content appears to be higher than expected. This curious phenomenon is classically met when the global chemical composition of a TaC-rich alloy is assessed by EDS: the TaC carbides emerging on the metallographic surface lead to the enhancement of the concentration in Ta. This phenomenon did not occur for the NTC10Cr alloy (and may be for the NTC20Cr one too). This one obviously contains much less TaC carbides than the other alloys.

About the microstructures, one can remark first that the matrix is unsurprisingly dendritic in all cases. Two types of particles are present: chromium carbides (the dark ones) and tantalum carbides (the white ones). The microstructure of the NCT30Cr alloy is rather well known. Indeed, the Ni(bal.)–30Cr–0.4C–6Ta alloy (contents in wt%) was many times characterized earlier (e.g., in [14]). One can easily recognize the Cr_7C_3 and TaC carbides, notably. Thus, thanks to the aspect similarities (morphology, tint), the dark particles and the white ones appearing in the NTC10Cr, NTC20Cr and NTC40Cr alloys can be identified as being Cr_7C_3 and TaC, respectively. In the first four alloys, one can also see that the peripheries of dendrites are particularly clear. This is due to tantalum segregation during solidification. This phenomenon, classical for such alloys, well helps to distinguish the dendritic structure of the matrix of the NTC10Cr alloy. The NTC50Cr alloy is particular since very dark areas coexist with the dendritic matrix and white areas.

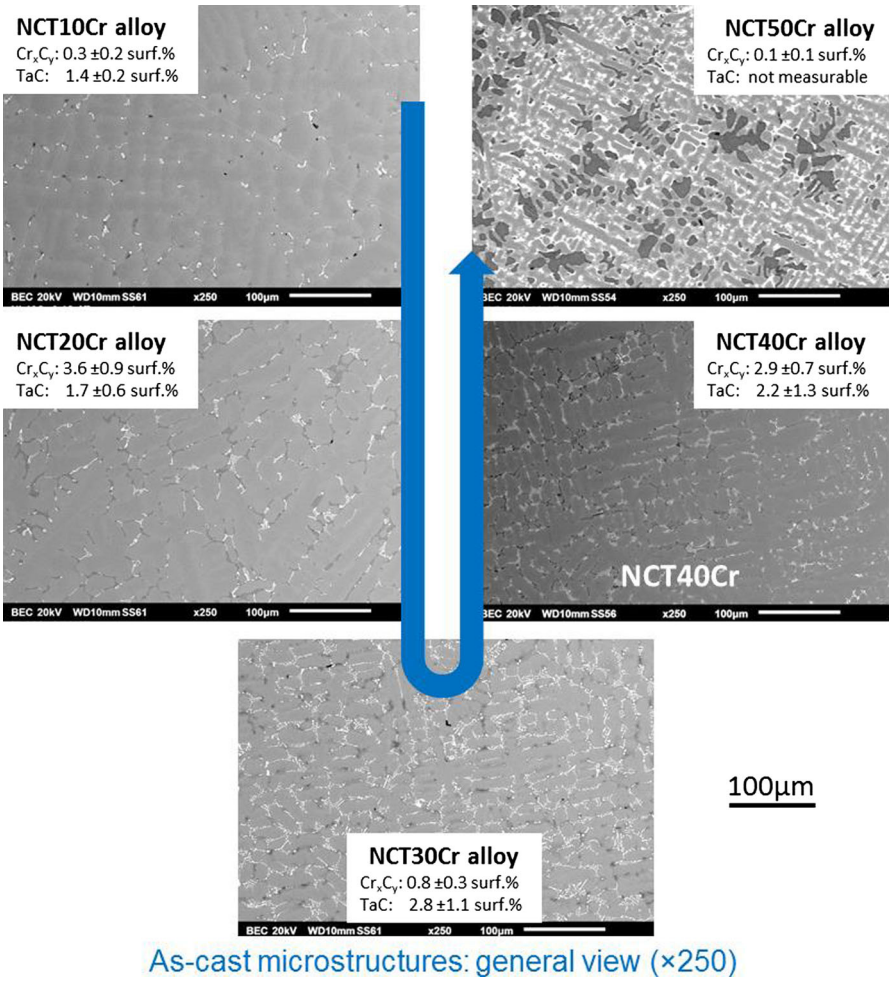

Fig. 1 As-cast microstructures of the five studied alloys (SEM/BSE micrographs, large view: ×250)

Table 2 Obtained chemical compositions for the five alloys (weight contents, 3 EDS full frame analyses)

Alloys	Ni	Cr	Ta	C[a]
"NCT10Cr"	Bal.	10.2 ± 0.3	5.9 ± 0.2	0.4
"NCT20Cr"	Bal.	19.8 ± 0.2	6.3 ± 0.1	0.4
"NCT30Cr"	Bal.	27.2 ± 0.5	10.1 ± 0.4	0.4
"NCT40Cr"	Bal.	40.3 ± 0.6	6.9 ± 0.5	0.4
"NCT50Cr"	Bal.	49.6 ± 0.6	6.6 ± 0.3	0.4

[a]Cannot be controlled; supposed to be well respected

These white areas are composed of dendrites peripheries rich in Ta (due to Ta segregation) and of tantalum carbides. The very dark areas are certainly the BCC Cr-based rich part of the matrix which was previously identified in a {Ta, C}-free

Ni–50Cr alloy [22] whose matrix structure is very similar to the NCT50Cr one. This can be verified, for the chemical composition point of view, in Table 3 which gives the results of EDS spot analysis of the two phases (last lines). According to these results, the gray dendrite centers contain more Ni than Cr (45–46 wt%Cr only) while the dark areas contain 60 wt%Cr and more.

In the top part of each micrograph presented in Fig. 1, one also gives the values of the surface fractions of the chromium carbides and of the tantalum carbides, except for the NCT50Cr alloy in which it was not possible to distinguish the tantalum carbides from the highly Ta-segregated peripheral zones of dendrites. These values are the average values and the standard deviation values calculated from three image analyses. One can see that the surface fraction of chromium carbides increases from the NCT10Cr alloy to the NCT20Cr one. It decreases when arriving to the NCT30Cr. It increases again for the NCT40Cr alloy and decreases again for the NCT50Cr alloy. At the same time, the surface fraction increases steadily from the NCT10Cr alloy to the NCT30Cr alloy and decreases when the Cr content keeps on increasing.

Detailed views of the microstructures of the five alloys after elaboration are given in Fig. 2. One can first observe the carbides in better condition. This allows discovering the eutectic origin of the chromium carbides: these ones are acicular and mixed with the peripheral parts of the matrix dendrites (NTC10Cr to NTC40Cr). The tantalum carbides are obviously also of a eutectic nature: script-like shaped and mixed with the outer part of the dendrites too (NTC10Cr to NTC30Cr). The white Ta-rich particles present in the interdendritic areas of the NTC40Cr alloy seem to be morphologically different from the eutectic TaC of the alloys which contain less chromium: they appear to be intermediate to the well-defined script-like-shaped TaC (alloys with Cr $\leq$ 30 wt%) and the more diffuse white interdendritic particles present in the NTC50Cr alloy. The spot analyses performed on the coarsest carbides found in the alloys seemed confirming the stoichiometries of the Cr_7C_3 carbides (NTC10Cr to NTC40Cr) and of the TaC ones (NTC10Cr to NTC50Cr). In contrast, no concluding result was obtained by this way for the Ta-rich white areas which are present in the NCT50Cr alloy, except the fact that it seems to be very rich in Ta.

Table 3 Obtained chemical compositions for the matrix in the as-cast alloys (weight contents, 3 EDS spot analyses)

Alloys	Ni	Cr	Ta	C
"NCT10Cr"	Bal.	10.0 ± 0.2	6.8 ± 1.2	Not measurable
"NCT20Cr"	Bal.	19.0 ± 0.3	4.6 ± 0.2	
"NCT30Cr"	Bal.	26.0 ± 0.1	6.4 ± 0.3	
"NCT40Cr"	Bal.	38.0 ± 0.2	3.8 ± 0.3	
"NCT50Cr"	Gray matrix	45.5 ± 0.3	3.8 ± 0.1	
	Black matrix	60.6 ± 0.9	3.1 ± 0.4	

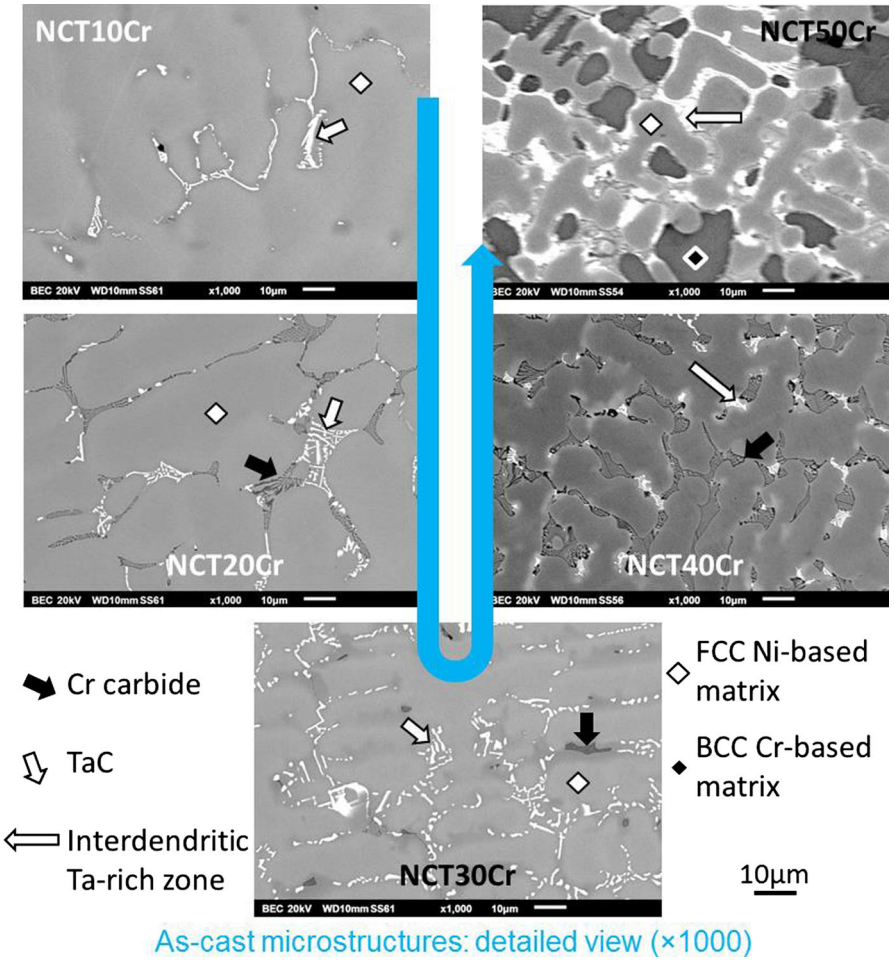

Fig. 2 As-cast microstructures of the five studied alloys (SEM/BSE micrographs, detailed view, ×1000)

Oxidation Result at 1127 °C

After 24 h spent at 1127 °C in the laboratory air, more or less complex oxide scales were present around the samples. Except for the two Cr poorest alloys (NCT10Cr and NCT20Cr) the external scale spalled off during the cooling. It was thus not always possible to extensively specify all the oxidation products. General views of the surface and subsurface deterioration seen in cross section are provided in Fig. 3 while more magnified micrographs can be consulted in Fig. 4. The NCT10Cr alloy was obviously covered by a mix of rather thin chromia (constituting the inner layer) and by a thicker complex oxide involving both nickel and chromium (constituting the outer layer). The alloy/external scale is very irregular. This suggests that oxidation was penetrating and that catastrophic oxidation was imminent. In the subsurface, but very close to the alloy/oxide scale interface, an almost continuous

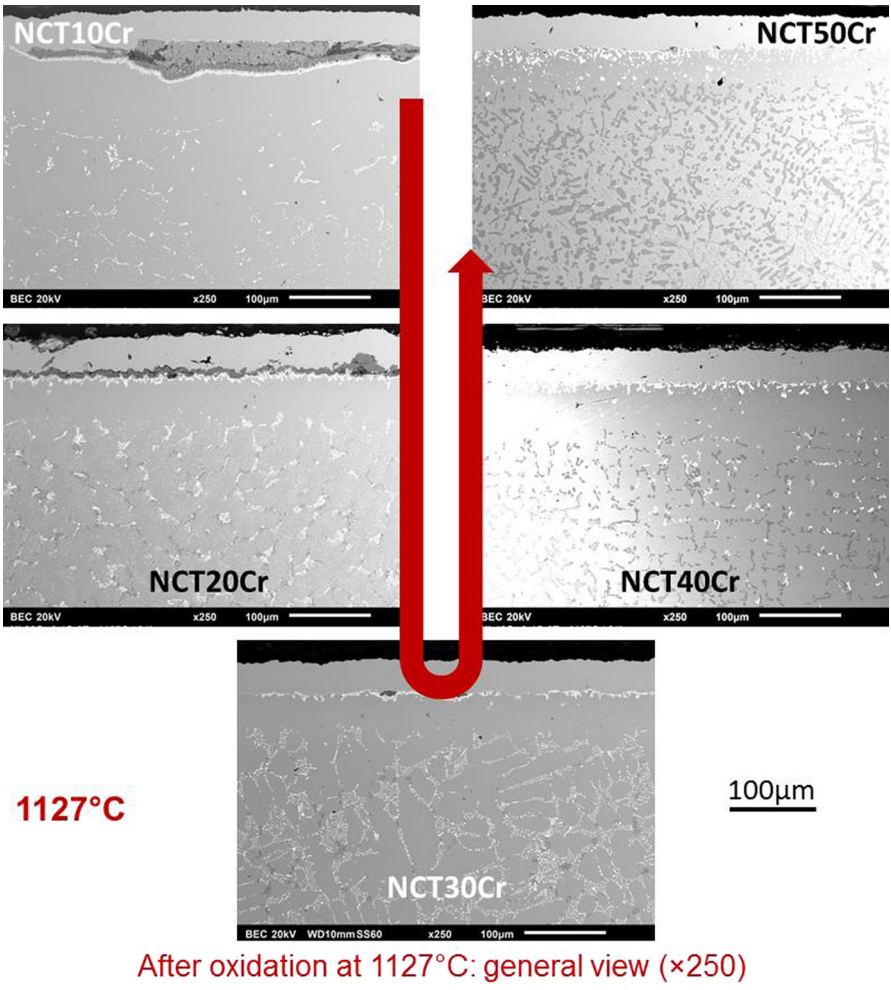

Fig. 3 Surface and subsurface states after oxidation at 1127 °C during 24 h (SEM/BSE micrographs, large view: ×250)

and rather compact complex oxide involving both chromium and tantalum was present. As soon as the chromium content in alloy is equal to 10 wt%Cr or higher, only chromia is present on the surface of the alloy. Chromia is very much present over the NCT20Cr, but just small chromia parts remain on surface for the NCT30Cr, NCT40Cr and NCT50Cr alloys. Just below, in the extreme surface part of alloy, the $CrTaO_4$ oxide is present in significant quantity, but more as juxtaposed oxides islands than an almost continuous subscale as for the NCT10Cr alloy. One can also notice that when the Cr content in alloy increases along this series, additional $CrTaO_4$ oxides appear to be also present in the whole carbide-free zone (NCT40Cr and NCT50Cr). In contrast, they only constitute the outer almost continuous oxide at the extreme surface of alloy for the NCT10Cr, NCT20Cr and NCT30Cr alloys.

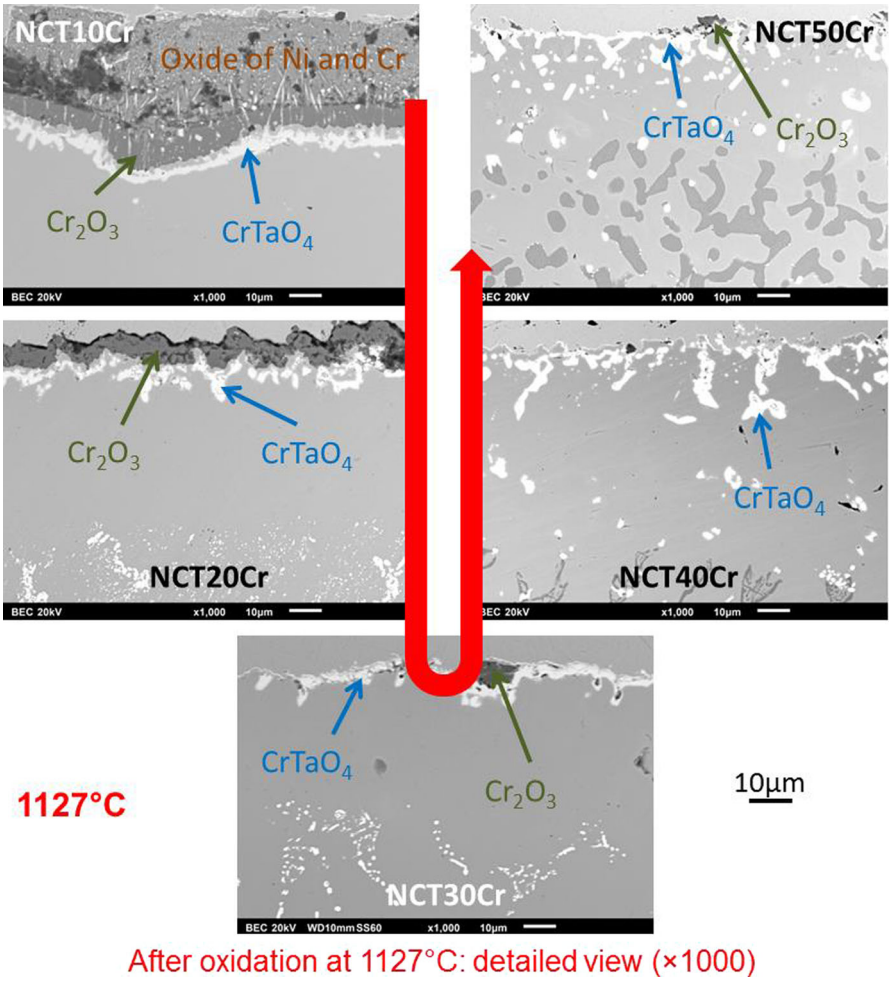

Fig. 4 Surface and subsurface states after oxidation at 1127 °C during 24 h (SEM/BSE micrographs, detailed view: ×1000)

One must say that, in the case of the NCT50Cr alloy, the outer alloy zone modified by oxidation is more a {BCC Cr-based phase}-free zone than a carbide-free zone as all the other alloys.

Obviously, the running development of a zone which is free of carbides (all alloys except NCT50Cr) or which is free of BCC Cr-based phase (NCT50Cr) demonstrates the diffusion of Cr and Ta toward the oxidation front (Fig. 5). SEM/EDS concentration profiles acquired perpendicularly to the oxidation front confirm that Cr diffusion and Ta diffusion occurred. These {Cr and Ta}-depleted depths tend to be deeper than the carbide-free zones, but the depths are of the same order of magnitude. The depth of the carbide-free zone depends on the alloy, as is to say on the initial alloy chromium content. It decreases from about 70 µm for NCT10Cr to

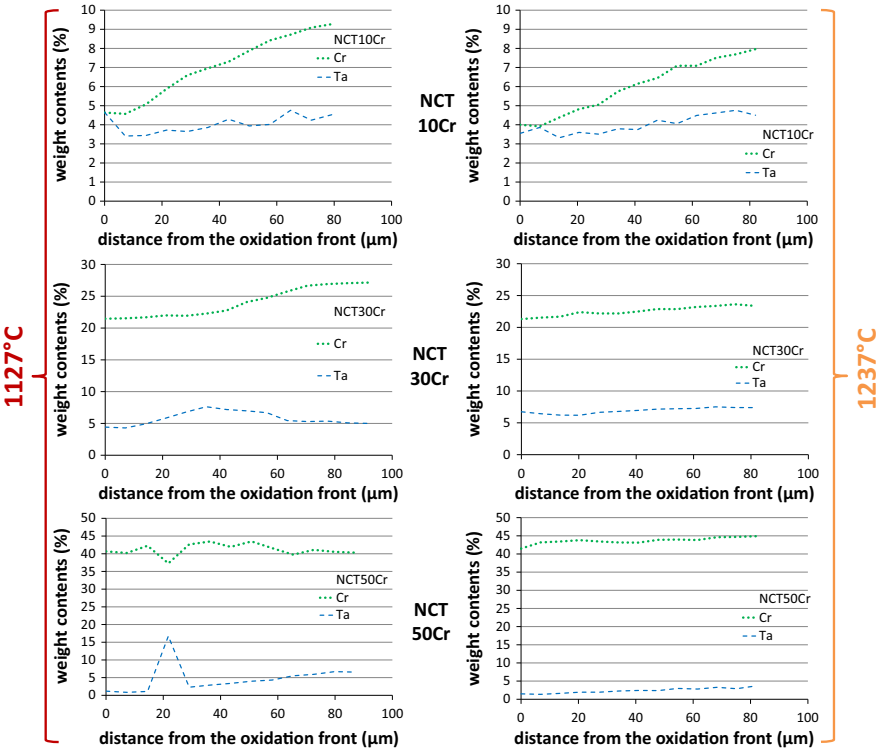

Fig. 5 Concentration profiles in the subsurfaces of three of the five alloys after oxidation at 1127 °C and at 1237 °C (SEM/EDS)

about 40 μm for NCT30Cr. It increases to 60 μm for NCT40Cr. In the case of NCT50Cr, the depth does not keep on increasing but it decreases, on the contrary. One must notice, for the later alloy, that what is significantly changed in the subsurface is not due to carbide dissolution but to the disappearance of the second phase of matrix (the BCC Cr-based one).

Table 4 Intervals of thickness values for the external oxide scale (first results column) and average ± standard deviation values of the carbide-free depth (second results column) for the five alloys oxidized for 24 h at 1127 °C

Alloys	Oxide scale thickness (μm)	Carbide-free zone depth (μm)
"NCT10Cr"	19–44	66.0 ± 9.0
"NCT20Cr"	7–20	49.3 ± 3.1
"NCT30Cr"	Spalled off	44.3 ± 4.3
"NCT40Cr"	Spalled off	57.9 ± 10.6
"NCT50Cr"	Spalled off	34.2 ± 4.9

Table 4 also shows few values of thickness of the external oxide scale. Measurement was possible only for the NCT10Cr and NCT20Cr alloys. These ones kept oxide scale parts in quantities high enough to permit thickness evaluation, in contrast with the other alloys which all lost their external oxide scales by spallation at cooling. Since the oxidation process was rather heterogeneous all along each surface, with as results very variable nature and thickness, only a tentative range of thickness is given. Oxidation induced Cr and Ta depletion for all alloys (examples in Fig. 5). The chromium content in extreme surface was assessed by three EDS spot analyses. The results (average ± standard deviation) are given in Table 5. For each alloy, the decrease in Cr content close to the alloy/external oxides interface was between 5 and 10 wt%. The local loss in Cr content continuously increases from the NCT20Cr alloy to the NCT50Cr alloy. The NCT10Cr does not obey this evolution because of its almost catastrophic oxidation.

Oxidation Result at 1237 °C

The metallographic exploitation of the samples oxidized at 1237 °C for the same duration of 24 h was driven similarly to the oxidation tests at 1127 °C, by:

- the observation of the cross sections at ×250 (Fig. 6) and ×1000 (Fig. 7),
- performing concentration profiles in the subsurface perpendicularly to the oxidation front (Fig. 5, graphs of the right side),
- the tentative measurement of the external oxide scale thickness (Table 6) when limited spallation at cooling did allow that,
- the measurement of the carbide-free depth (Table 6)
- and the measurement of the chromium content in extreme surface (Table 7).

The results and observations were globally the same as for the samples oxidized at 1127 °C: start of catastrophic oxidation for the Cr lowest alloy (NCT10Cr), local high thickness of the external scale, very irregular alloy/scale frontier, presence of many types of oxides, minimum of carbide-free depth for the NCT30Cr alloy, existence of a {BCC Cr phase}-free subsurface for the NCT50Cr alloy, same type of

Table 5 Average and standard deviation for the chromium content in alloy close to the interface with the external oxide (3 EDS spot analyses)

Alloys (24 h 1127 °C)	Chromium content in extreme surface (wt%)	Difference to the initial Cr content (wt%)
"NCT10Cr"	4.8 ± 0.3	− 5.4
"NCT20Cr"	15.5 ± 1.3	− 4.3
"NCT30Cr"	21.6 ± 0.1	− 5.6
"NCT40Cr"	33.2 ± 0.1	− 7.1
"NCT50Cr"	41.1 ± 1.1	− 8.5

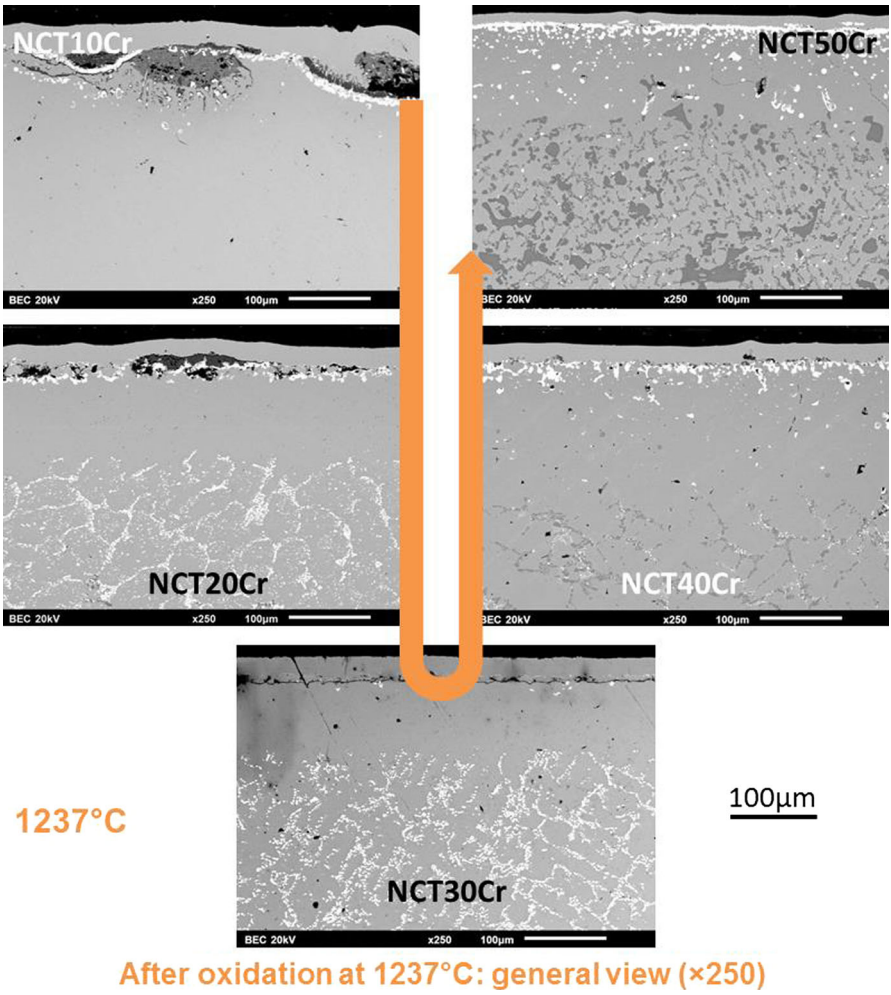

Fig. 6 Surface and subsurface states after oxidation at 1237 °C during 24 h (SEM/BSE micrographs, large view: ×250)

evolution of the Cr loss in extreme surface from the NCT10Cr alloy to the NCT50Cr one, and same types of Cr and Ta concentration profiles.

Thus, the differences between the two temperatures are not qualitative, but they are quantitative: thicker external oxide scales and deeper carbide-free (or BCC Cr phase-free) zones. The chromium contents in extreme surface do not depend on temperature for a given alloy (Fig. 8), the better Cr diffusion easiness offsetting the higher Cr consumption.

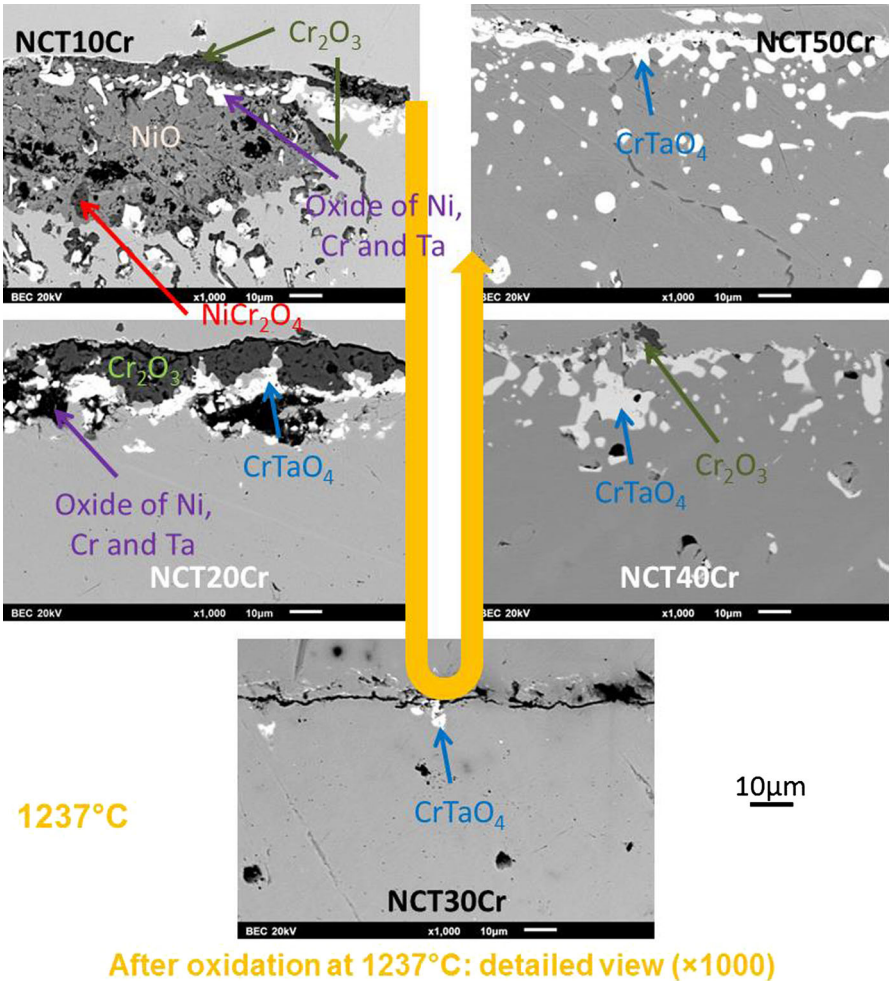

Fig. 7 Surface and subsurface states after oxidation at 1237 °C during 24 h (SEM/BSE micrographs, detailed view: ×1000)

Discussion

Concerning the effect of the modification of the Cr content on the natures and proportions of the obtained carbides in cast alloys, looking to the SEM/BSE micrographs allowed first feeling that the variation of the chromium content in the chemical composition of the alloys had consequences on the carbides population of the as-cast alloys. Image analysis allowed confirming these trends by quantitative results. The lowest Cr content tested here, 10 wt%Cr, led to a lowering of the chromium carbides quantity but curiously also of the tantalum carbide ones. Adding 10 wt%Cr more induced a logical increase in chromium carbides but also in tantalum carbides. Repeating this addition to reach 30 wt%Cr led to a maximal

Table 6 Intervals of thickness values for the external oxide scale (first results column) and average ± standard deviation values of the carbide-free depth (second results column) for the five alloys oxidized for 24 h at 1237 °C

Alloys	Oxide scale thickness (μm)	Carbide-free zone depth (μm)
"NCT10Cr"	17–160	> 300
"NCT20Cr"	11–15	105 ± 5
"NCT30Cr"	Spalled off	87 ± 6
"NCT40Cr"	Spalled off	170 ± 13
"NCT50Cr"	Spalled off	101 ± 6

Table 7 Average and standard deviation for the chromium content in alloy close to the interface with the external oxide (3 EDS spot analyses)

Alloys (24 h 1237 °C)	Chromium content in extreme surface (wt%)	Difference to the initial Cr content (wt%)
"NCT10Cr"	4.1 ± 0.2	− 6.1
"NCT20Cr"	14.5 ± 0.3	− 5.3
"NCT30Cr"	21.5 ± 0.2	− 5.7
"NCT40Cr"	33.7 ± 0.1	− 6.6
"NCT50Cr"	42.7 ± 1.1	− 6.9

fraction in TaC carbides and to the rarefaction of the chromium carbides. Choosing a 40 wt%Cr content let the TaC fraction stationary, but it favors the formation of more chromium carbides than for 30 wt%Cr. One can suspect a solid solution effect in a first time (sufficient available place for the greatest part of chromium and tantalum in the NCT10Cr alloy) and thereafter new balance between solid solution and carbides when Cr is more present in the chemical composition, with a singular effect in the case of the NCT30Cr alloy in which the chromium tends to stay preferentially in solid solution and to promote the formation of more TaC carbides.

Concerning the oxidation point of view, one can start by reminding that it was earlier observed that the Ni–30Cr–0.4C–6Ta alloy, serving as base for this work, was well oxidation resistant at high temperature. However, one must also remind that it presented a high tendency to oxide spallation in thermal cycling. Concerning the strengthening particles for potential high temperature mechanical properties, this alloy presented the problem of co-precipitation of primary tantalum carbides and chromium carbides, despite that the weight contents in C and Ta were chosen to obtain equal atomic contents for these two carbide-forming elements. This molar equivalence of Ta and C was a recipe which was nonetheless efficient for cobalt-based and iron-based alloys. Thanks to its good behavior in isothermal oxidation, it was permitted to envisage to decrease the Cr content in order to promote the precipitation of more TaC at the expense of the chromium carbides.

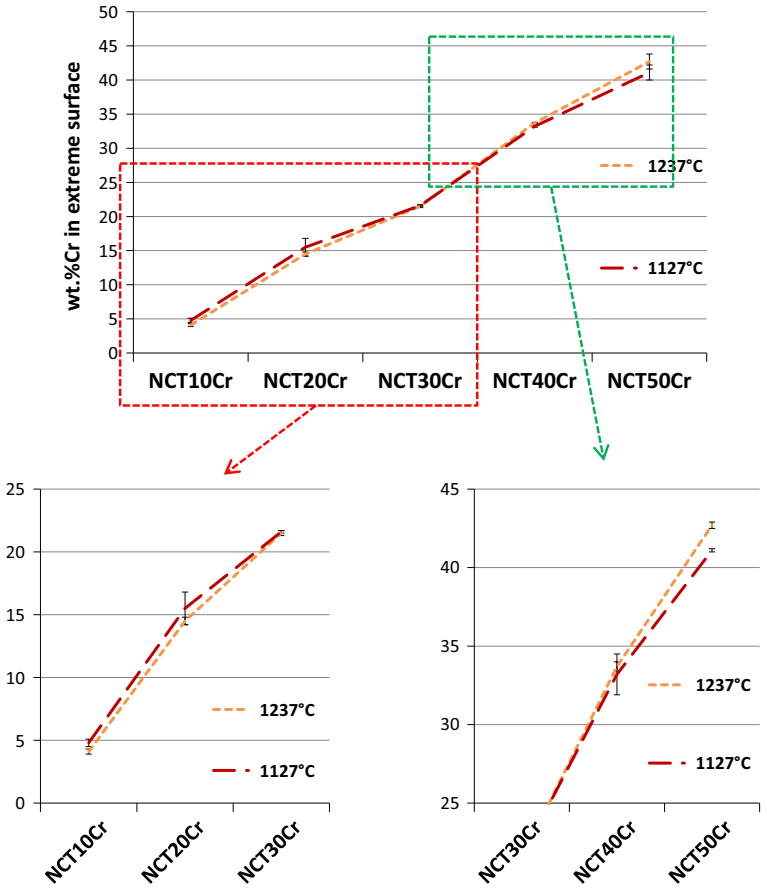

Fig. 8 Comparison between the chromium content in extreme surface after 24 h of oxidation at 1127 °C and at 1237 °C (SEM/EDS)

In these alloys, chromium is the most important element for the high-temperature oxidation behavior. Its content was here either too low to allow good resistance (the 10 wt%Cr contained in the NCT10Cr alloy) or sufficiently high (30 wt% and beyond). The 20 wt%Cr-containing alloy (NCT20Cr) seems to well behave at the two test temperatures, but it is possible that this behavior may degenerate for durations higher than 20 h. This is suggested by the not perfect compactness and regularity of the chromia scale: after 24 h at 1127 or 1237 °C this chromia scale contains porosities and is a little wavy because of the possible start of inward oxidation. It is possible that this wavy shape of the external chromia scale favored its adherence on the substrate. Indeed, the chromia scale had much less spalled off than for the Cr-rich alloys. Concerning spallation, only the alloys with irregular alloy/oxide-scale interface were resistant against this phenomenon during cooling. Indeed, the NCT30Cr, NCT40Cr and NCT50Cr all lost the main part of their external oxides. It was thought earlier [21] that tantalum oxide which formed just

under the chromia scale may threaten the adherence of chromia on substrate. This was found again here for the alloys containing between 30 and 50 wt%Cr which displayed both a very regular alloy/oxide-scale interface and an almost continuous suboxide of $CrTaO_4$. The deleterious effect of the $CrTaO_4$ sublayer on the adherence of chromia may be explained by the mismatch of crystalline network between chromia (eskolaite) which possesses a corundum crystal structure (with Cr^{III} replacing Al^{III} at the same locations in the crystal) and the rutile structure of $CrTaO_4$ [24, 25]. Classically encountered in case of high Ta contents (5–9 wt%) in polycrystalline [26], directionally solidified [27] and single-crystalline [28] nickel-based superalloys, it was reported that tantalum often leads to the formation of more or less continuous sublayers of $CrTaO_4$ during high-temperature oxidation. This starts rather early and progresses with the growth or coarsening of the subsurface $CrTaO_4$ islands together with the deepening of the TaC-free zone. The coalescence of these coarsening subsurface oxides progressively results in an almost continuous $CrTaO_4$ sublayer. Consequently to the formation of this oxide of both chromium and tantalum, severe spallation of the chromia external scale during post-oxidation cooling was systematically observed for Ta-rich nickel-based, cobalt-based, iron-based and {iron, nickel}-based polycrystalline cast alloys [30–32].

In all cases, Cr diffused toward the oxidation front, from the solid solution matrix, the dissolving chromium carbides or the disappearing BCC Cr phase. The two latter acted as important Cr reservoirs, depending on the alloy. Tantalum diffused too from the solid solution matrix and from the tantalum carbides which are important Ta reservoirs too. One well knows the consequence for chromium: formation and maintenance of a protective chromia scale. Contrariwise, for Ta and its oxide, one does not know if its formation, obviously detrimental for the adherence of the external oxide, may act as a supplementary protection against oxidation, added to the one by chromia. It is true that the NCT10Cr alloy, although threatened here and there by a possible local catastrophic oxidation, rather resisted oxidation even at 1237 °C, perhaps helped by the subsurface continuous $CrTaO_4$ oxide. This merits to be deeper studied. Solutions for combatting the oxide spallation problem must be found, why not by an yttrium addition allowing the pegging of the external scale.

Conclusion

Decreasing the Cr content of the Ni–30Cr–O.4C–6Ta base (wt%) induced a visible lowering of the oxidation resistance at the two studied temperatures as soon as the alloy contains only 10 wt%Cr. But the oxidation was not catastrophic of a general manner, at least after 24 h of exposure to air. It is possible that Ta was responsible of the limitation of the detrimental effect of the Cr lowering down to a so low content. But this Cr decrease did not induce the expected effect, as is to say the stabilization of the TaC carbides known to be very favorable to mechanical strength at elevated temperature. Curiously, but a possible explanation was presented here, this is by increasing the Cr content that one obtains more TaC carbides with few chromium carbides. Since this effect was accompanied by a better resistance against

high-temperature isothermal oxidation, the way to follow is progressively increasing the Cr content beyond the usual 30 wt%Cr, but not too high to avoid the appearance of the BCC Cr phase which can be supposed to mechanically weaken the alloy. The optimal Cr content remains to be found and the oxidation and creep behaviors to be specified.

References

1. P. Kofstad, *High Temperature Corrosion*, (Elsevier Applied Science, Amsterdam, 1988).
2. D. Young, *High Temperature and Corrosion of Metals*, (Elsevier, Amsterdam, 2008).
3. C. T. Sims and W. C. Hagel, *The Superalloys*, (Wiley, Hoboken, 1972).
4. E. F. Bradley, *Superalloys: A technical guide*, (ASM International, Metals Park, 1988).
5. N. Birks, G. H. Meier and F. S. Pettit, *Introduction to the High-Temperature Oxidation of Metals*, 2nd ed, (Cambridge University Press, Cambridge, 2009).
6. S. Langard, *Biological and Environmental Aspects of Chromium*, (Elsevier Science, Amsterdam, 1983).
7. D. Caplan and M. Cohen, *Journal of the Electrochemical Society* **108**, (5), 1961 (438).
8. P. Berthod, *Oxidation of Metals* **64**, (3–4), 2005 (235).
9. G. C. Wood, I. G. Wright, T. Hodgkiess and D. P. Whittle, *Werkstoffe und Korrosion* **21**, 1970 (900).
10. N. Mu, K. Jung, N. M. Yanar, F. S. Pettit, G. R. Holcomb, B. H. Howard and G. H. Meier, *Oxidation of Metals* **79**, 2013 (461).
11. G. R. Holcomb and D. E. Halman, *Scripta Metarialia* **54**, 2006 (1821).
12. S. R. J. Saunders, M. Monteiro and F. Rizzo, *Progress in Materials Science* **53**, 2008 (775).
13. P. Berthod, L. Aranda, S. Mathieu and M. Vilasi, *Oxidation of Metals* **79**, (5–6), 2013 (517).
14. P. Berthod, L. Aranda, C. Vébert and S. Michon, *Calphad* **28**, (2), 2004 (159).
15. M. J. Donachie and S. J. Donachie, *Superalloys: A Technical Guide*, 2nd ed, (ASM International, Materials Park, 2002).
16. S. Michon, L. Aranda, P. Berthod and P. Steinmetz, *La Revue de Métallurgie – C.I.T./Science et Génie des Matériaux* **9**, 2004 (651).
17. P. Berthod, *Advanced Materials Letters* **8**, (8), 2017 (866).
18. P. Berthod, *Advances in Materials Science and Engineering*, article ID 4145369, https://doi.org/10.1155/2017/4145369 (2017)
19. L. Corona, E. Conrath, P. Berthod, M. Ritouet, in proceedings of the International Conference on Sustainable Energy and Information Engineering (SEEIE 2016) 442–446.
20. J. Di Martino, S. Michon, L. Aranda, P. Berthod, R. Podor and C. Rapin, *Annales de Chimie – Sciences des Matériaux* **28**, (Suppl. 1), 2003 (S231).
21. P. Berthod, C. Vébert and L. Aranda, *Journal of Materials Science* **42**, 2007 (352).
22. E. Conrath and P. Berthod, *Materials at High Temperature* **33**, (2), 2016 (189).
23. H.-T. Lin, J. Hemrick, M. Singh and A. Michaelis, *Advanced and Refractory Ceramics for Energy Conservation and Efficiency*, (Wiley, Hoboken, 2015).
24. P. Massard, J.-C. Bernier and A. Michel, *Journal of Solid State Chemistry* **4**, 1972 (269).
25. M. A. Tena, M. Llusar, J.-A. Badenes, M. Vicente and G. Monros, *British Ceramic Transactions* **99**, (5), 2000 (219).
26. S.-J. Park, S.-M. Seo, Y.-S. Yoo, H.-W. Jeong and H. Jang, *Corrosion Science* **90**, 2015 (305).
27. W. Ren, F. Ouyang, B. Ding, Y. Zhong, J. Yu, Z. Ren and L. Zhou, *Journal of Alloys and Compounds* **724**, 2017 (565).
28. J. A. Nychka, D. R. Clarke and G. H. Meier, *Materials Science and Engineering A* **490**, 2008 (359).
29. P. Berthod, S. Raude, A. Chiaravalle, A.-S. Renck, C. Rapin and R. Podor, *La Revue de Métallurgie – C.I.T./Science et Génie des Matériaux* **12**, 2004 (1031).
30. P. Berthod, L. Aranda and C. Vébert, *Annales de Chimie-Science des Matériaux* **31**, (2), 2006 (213).
31. P. Berthod, S. Raude and A. Chiaravalle, *Annales de Chimie-Science des Matériaux* **31**, (2), 2006 (237).
32. P. Berthod, Y. Hamini and L. Aranda, *Materials Science Forum* **595–598**, 2008 (861).